International Journal of Nanomedicine

Dovepress
open access to scientific and medical research

Open Access Full Text Article

ORIGINAL RESEARCH

An efficient Trojan delivery of tetrandrine by poly(N-vinylpyrrolidone)-block-poly(ε-caprolactone) (PVP-b-PCL) nanoparticles shows enhanced apoptotic induction of lung cancer cells and inhibition of its migration and invasion

This article was published in the following Dove Press journal:
International Journal of Nanomedicine
27 December 2013
Number of times this article has been viewed

Huae Xu[1,2]
Zhibo Hou[3]
Hao Zhang[4]
Hui Kong[2]
Xiaolin Li[4]
Hong Wang[2]
Weiping Xie[2]

[1]Department of Pharmacy, [2]Department of Respiratory Medicine, The First Affiliated Hospital of Nanjing Medical University, Nanjing, People's Republic of China; [3]First Department of Respiratory Medicine, Nanjing Chest Hospital, Nanjing, People's Republic of China; [4]Department of Geriatric Gastroenterology, The First Affiliated Hospital of Nanjing Medical University, Nanjing, People's Republic of China

Correspondence: Hong Wang; Weiping Xie
Department of Respiratory Medicine, The First Affiliated Hospital of Nanjing Medical University, 300# Guangzhou Road, Nanjing 210029, People's Republic of China
Tel +86 25 68 136 580; +86 25 68 136 379
Email hongwang@njmu.edu.cn; wpxie@njmu.edu.cn

Abstract: Earlier studies have demonstrated the promising antitumor effect of tetrandrine (Tet) against a series of cancers. However, the poor solubility of Tet limits its application, while its hydrophobicity makes Tet a potential model drug for nanodelivery systems. We report on a simple way of preparing drug-loaded nanoparticles formed by amphiphilic poly(N-vinylpyrrolidone)-block-poly(ε-caprolactone) (PVP-b-PCL) copolymers with Tet as a model drug. The mean diameters of Tet-loaded PVP-b-PCL nanoparticles (Tet-NPs) were between 110 nm and 125 nm with a negative zeta potential slightly below 0 mV. Tet was incorporated into PVP-b-PCL nanoparticles with high loading efficiency. Different feeding ratios showed different influences on sizes, zeta potentials, and the drug loading efficiencies of Tet-NPs. An in vitro release study shows the sustained release pattern of Tet-NPs. It is shown that the uptake of Tet-NPs is mainly mediated by the endocytosis of nanoparticles, which is more efficient than the filtration of free Tet. Further experiments including fluorescence activated cell sorting and Western blotting indicated that this Trojan strategy of delivering Tet in PVP-b-PCL nanoparticles via endocytosis leads to enhanced induction of apoptosis in the non-small cell lung cancer cell A549 line; enhanced apoptosis is achieved by inhibiting the expression of anti-apoptotic Bcl-2 and Bcl-xL proteins. Moreover, Tet-NPs more efficiently inhibit the ability of cell migration and invasion than free Tet by down-regulating matrix metalloproteinases (MMP)-2 and MMP-9, as well as up-regulating tissue inhibitor of MMP-3 (TIMP-3). Therefore, data from this study not only confirms the potential of Tet in treating lung cancer but also offers an effective way of improving the anticancer efficiency of Tet by nanodrug delivery systems.

Keywords: tetrandrine, poly(N-vinylpyrrolidone), lung cancer, nanoparticles

Introduction

Lung cancer, one of the most serious respiratory diseases, is the most common cause of cancer-related deaths around the world.[1,2] This poor prognosis is due to its highly invasive and metastatic characteristics, with a large amount of patients undergoing tumor cell invasion and migration before diagnosis.[3,4]

Tetrandrine (Tet), a bis-benzylisoquinoline alkaloid isolated from the root of hang-fang-chi (*Stephania tetrandra* S Moore), has been shown to have antitumor effects against several cancers.[5–8] In previous reports, Tet was found to not only to inhibit the growth of tumors, but it also showed its potential in increasing the sensitivity of chemotherapy.[9–12]

It is known that the balance between extracellular matrix (ECM) deposition and degradation is essential for preventing carcinogenesis.[13,14] Matrix metalloproteinases (MMPs), whose activity can be inhibited by tissue inhibitor of MMP type three (TIMP-3), contribute to the metastasis of tumors primarily by degrading a major component of cell membrane, type IV collagen.[15] Tet also displays an inhibitory effect on tumor metastasis in several cancer cell lines.[16,17] Therefore, the ability of Tet to inhibit the growth and metastasis of tumor makes it a promising drug in cancer treatment.

However, Tet's poor solubility limits its application, while its hydrophobicity makes Tet a promising model drug for nanodelivery systems. Several studies have reported the encapsulation of Tet into liposomes or nanoparticles.[18–20] For example, Tet-loaded magnetic Fe_3O_4 nanoparticles could induce apoptosis and reverse multidrug resistance in leukemic cells.[21,22] Another study reported that Tet-loaded poly(ethylene glycol)-b-polycaprolactone (mPEG-PCL) nanoparticles could reverse pH-induced physiological drug resistance in vitro and in vivo.[23] In our previous studies, Tet-loaded mPEG-PCL nanoparticles showed an antitumor effect in several gastrointestinal cancer cell lines.[24–26] We demonstrated that Tet-loaded mPEG-PCL nanoparticles showed enhanced antitumor efficiency compared to free Tet through more efficient penetration of cell membrane by endocytosis.[25]

Recently the application of nanoparticle systems in tumor imaging and therapy has attracted more and more interest.[27–31] Amphiphilic polymeric nanoparticles with polyethylene glycol (PEG) as a drug carrier show potential in delivering drugs to tumors. However, it has been reported that PEG fails to completely avoid uptake by macrophages and still partially activates complement systems, which leads to a shorter circulation time.[32] Therefore, water-soluble poly(N-vinylpyrrolidone) (PVP), which is used in many drug delivery systems, is chosen as an alternative option to PEG.[33,34] In our previous studies, PVP modification could lengthen the in vivo circulation time of nanoparticles due to a more effective escape from macrophage systems.[35] Therefore, the drug-loaded nanoparticles could be considered a "Trojan horse" designed to deliver anticancer drugs. When the nanoparticles are incubated with cancer cells, they are then transferred into the cells through a process called endocytosis, thereby releasing the loaded drugs directly into the cell interior.[25]

Though Tet is reported to inhibit the metastasis of some tumors, there is little evidence of the anti-metastatic effect of Tet-loaded nanoparticles. In our current study we employ poly(N-vinylpyrrolidone)-block-poly(ε-caprolactone) (PVP-b-PCL) as a drug carrier. Here we characterized Tet-loaded PVP-b-PCL nanoparticles (Tet-NPs) with different feeding ratios and further studied differential apoptotic induction between Tet-NPs and Tet in A549 cells. In addition, wound scratch and Transwell assays were performed to evaluate the anti-migration and invasion ability of Tet-NPs; relative protein expression was then measured to further elucidate the possible mechanism underlying the superior antitumor effect of Tet-NPs. According to the results, we propose the hypothesis that delivery of Tet via PVP-b-PCL nanoparticles might effectively promote apoptosis and inhibit the migration and invasion of A549 cells, which could be a promising anticancer therapeutic strategy in treating lung cancer.

Materials and methods

Materials

Tet and acridine orange (AO) was purchased from Sigma-Aldrich (St Louis, MO, USA). Human non-small cell lung cancer cell line A549 was obtained from the Shanghai Institute of Cell Biology (Shanghai, People's Republic of China). Cell culture material (eg, RPMI 1640, fetal bovine serum) was obtained from Life Technologies (Carlsbad, CA, USA). All other chemicals were of analytical grade and used without further purification.

Methods

Formulation of nanoparticles

PVP-b-PCL was synthesized by ring-opening polymerization as described in our previous reports.[25,35] Tet-NPs were prepared by a nanoprecipitation method as described previously, with minor modification.[14,36] Briefly, a predetermined amount of PVP-b-PCL copolymers and Tet were dissolved in acetone. The obtained organic solution was added dropwise into ten times the volume of distilled water under gentle stirring and at room temperature. The solution was dialyzed in a dialysis bag (molecular weight cutoff 3,500) to remove acetone thoroughly. The resulting bluish aqueous solution was filtered through a 0.22 μm filter membrane to remove non-incorporated drugs. Drug-free nanoparticles were produced in a similar manner without adding drugs. Solutions of drug-loaded nanoparticles and empty nanoparticles were then lyophilized for further utilization.

Characterization of nanoparticles

Mean diameter and size distribution were measured before lyophilization by photon correlation spectroscopy (dynamic light scattering [DLS]) using a Brookhaven BI-9000 AT instrument (Brookhaven Instruments Corporation, Holtsville, NY, USA). Zeta potential was measured by the laser Doppler

anemometry (Zeta Plus, Zeta Potential Analyzer; Brookhaven Instruments Corporation).

Drug loading content (DLC) and encapsulation efficiency (EE)

The concentration of Tet was assayed on a Shimadzu LC-10 AD (Shimadzu Corporation, Kyoto, Japan) high-performance liquid chromatography (HPLC) system equipped with a Shimadzu ultraviolet (UV) detector and an Agilent C18, 5 μm, 200 mm × 4.6 mm reverse phase (RP)-HPLC analytical column (Agilent Technologies, Santa Clara, CA, USA). The mobile phase consisted of methanol (spectral grade, Merck KGaA, Darmstadt, Germany)/double-distilled water/ethylamine (90/10/0.05, v/v/v) pumped at a flow rate of 1.0 mL/minute with a determination wavelength of 282 nm. The concentration of Tet was determined based on the peak area at the retention time of 4.83 minutes by reference to a calibration curve. The following equations were applied to calculate the drug loading content (Equation 1) and encapsulation efficiency (Equation 2).

$$\text{Drug loading content (\%)} = \frac{\text{Weight of the drug in nanoparticles}}{\text{Weight of the nanoparticles}} \times 100 \quad (1)$$

$$\text{Encapsulation efficiency (\%)} = \frac{\text{Weight of the drug in nanoparticles}}{\text{Weight of the feeding drugs}} \times 100 \quad (2)$$

In vitro release of Tet-loaded nanoparticles

For in vitro release detection, 10 mg lyophilized Tet-loaded nanoparticles were suspended in 1 mL of 0.1 M phosphate buffered saline (PBS, PH 7.4). The solution was then placed into a pre-swelled dialysis bag with a 12 kDa molecular weight cutoff (Sigma-Aldrich) and immersed into 20 mL of 0.1 M PBS, pH 7.4, at 37°C with gentle agitation. One mL samples were withdrawn from the incubation medium and measured for Tet concentration as described above. After sampling, an equal volume of fresh PBS was immediately added into the incubation medium. The concentration of Tet released from the nanoparticles was expressed as a percentage of the total Tet in the nanoparticles and plotted as a function of time.

Nanoparticle uptake by A549 cells

Coumarin-6 was utilized as a fluorescent marker to assess the efficiency of nanoparticle uptake by tumor cells. About 5×10^5 A549 cells were seeded in six well plates with RPMI 1640 supplemented with 10% calf blood serum, and allowed to adhere at 37°C with 5% CO_2 for 24 hours prior to the assay. The medium was then replaced with 10 mL fresh RPMI 1640 containing coumarin-6 loaded nanoparticles (indicated by a dose of coumarin-6 at a concentration of 1 μg/mL). After 2 hours of incubation, the cell monolayers were rinsed three times with PBS buffer to remove excess nanoparticles. The cells were viewed and imaged under a fluorescence microscope (Eclipse E-800; Nikon Corporation, Tokyo, Japan) using a FITC (fluorescein isothiocyanate) filter with an excitation wavelength of 495 nm and emission wavelength of 517 nm (magnification =400×).

Cells were incubated for 2 hours, with or without the presence of 20 mM sodium azide (NaN_3), and collected for a quantitative analysis of nanoparticle uptake, as indicated by coumarin-6 content. The cell lysates were reconstituted in 500 μL of methanol and sonicated for 30 seconds at 5 Hz to extract the fluorescent dye from the nanoparticles. The samples were centrifuged at 12,000 rpm and 4°C for 10 minutes, and 400 μL of the supernatants were collected for HPLC analysis. The concentration of coumarin-6 was assayed on a Shimadzu LC-10 AD (Shimadzu Corporation) HPLC system equipped with a Shimadzu fluorescence detector (Model RF-10 AXL; Ex(λ) 450 nm/Em(λ) 490 nm; Shimadzu Corporation) and an Agilent C18, 5 μm, 200 mm × 4.6 mm RP-HPLC analytical column. The mobile phase consisted of spectral grade acetonitrile (Merck KGaA)/double-distilled water/1-heptane sulfonic acid sodium salt (65/35/0.005, v/v/v) pumped at a flow rate of 1.0 mL/minute. The concentration of coumarin-6 was determined based on the peak area by reference to a calibration curve. The efficiency of nanoparticle uptake was calculated from the amount of coumarin-6 detected in the cell and total added.

AO staining

A549 cells were treated with Tet or Tet-NPs at the equivalent concentration of 4 μg/mL for 48 hours, and then washed once in PBS, followed by fixation in cold methanol:acetone (1:1) for 5 minutes. After washing twice in PBS for 5 minutes, these cells were stained with AO (1 mL of a 1% stock concentration of AO in distilled water) at room temperature and immediately examined by fluorescence microscopy using filters for FITC (Eclipse E-800; Nikon, Tokyo, Japan) with an excitation wavelength of 490 nm and emission wavelength of 519 nm (magnification =400×).

Flow cytometry analysis

To conduct further quantitative analysis of apoptosis, the cells were treated with different doses of Tet or Tet-NPs

(1, 2, and 4 μg/mL) for 48 hours and then stained with annexin V-fluorescein isothiocyanate (FITC) and propidium iodide (PI) using the annexin V-FITC kit (eBioscience, Inc, San Diego, CA, USA). The cells were then subjected to flow cytometry according to the manufacturer's instructions and the stained cells were analyzed using a FACScan flow cytometer (Becton, Dickinson and Company, Franklin Lakes, NJ, USA).

Western blot analysis

The extraction of proteins from cells and Western blot analyses were performed as described in our previous reports. Primary antibodies used include rabbit anti-Bcl-2, anti-Bcl-xL, anti-MMP-2, anti-MMP-9, anti-TIMP-3 (Cell Signaling Technology, Inc, Danvers, MA, USA) and anti-β-actin (Sigma-Aldrich). Goat anti-rabbit horseradish peroxidase (HRP)-conjugated secondary antibody was purchased from Vector Laboratories Inc. (Burlingame, CA, USA). Cells were treated with Tet or Tet-NPs at an equivalent dose of 4 μg/mL for 48 hours. Bands were quantified using densitometric image analysis software (Quantity One, Bio-Rad, Hercules, CA, USA).

In vitro wound scratching assay

Cell migration was assayed using an in vitro wound scratching assay. A549 cells were plated into the 6-well plates and cultured in an incubator until confluent monolayers were formed. The cells were serum-starved for 12 hours and then a 'wound' (clear space) was made using a sterile pipette tip. At this time point (t=0 hours) wound margins were observed using phase contrast microscopy and photographed. Then, serum-free medium containing different doses of Tet or Tet-NPs (1, 2, and 4 μg/mL) was added to the plates and the cells were incubated for up to 48 hours at 37°C. The same fields of the wound margin were photographed at 24 and 36 hours. Pictures were superposed using Photoshop (Adobe Systems Incorporated, San Jose, CA, USA) and areas were measured using Scion Image Analysis Software (Scion Corporation, Frederick, MD, USA). The wound healing rate was calculated according to the following formula: (the average area of wound at 0 hours – the average area of wound at 24 or 48 hours)/the average area of wound in 0 hours. Experiments were repeated at least three times.

In vitro Transwell invasion assays

Invasion assays were performed in 24-well Transwell chambers (Corning Incorporated, Corning, NY, USA) containing polycarbonate filters with 8 μm pores coated with Matrigel (Becton, Dickinson and Company). Briefly, A549 cells were allowed to grow to subconfluency and were serum-starved for 24 hours. After detachment with trypsin, the cells were washed with PBS, resuspended in serum-free medium, and 2×10^4 cells were added to the upper chamber. Complete medium was added to the bottom chamber as a chemoattractant. Then, different doses of Tet or Tet-NPs (1, 2, and 4 μg/mL) was added to the inside of each insert and incubated for 48 hours in a cell culture incubator. Uninvaded cells on the upper surface of the filter were mechanically removed with a cotton swab, and the invasive cells on the lower membrane surface were fixed with methanol and stained with 0.1% crystal violet. The invading cells were counted and photographed under a microscope at 200× magnification. Five fields were counted per filter in each group and the experiment was conducted in triplicate.

Statistical analysis

Data were expressed as the mean ± standard deviation (SD) of three independent experiments. Statistical analysis for the comparison of relative groups was based on Student's t-test or one-way analysis of variance (ANOVA) with SPSS 11.5 software (IBM Corporation, Armonk, NY, USA). Significance was accepted at the 0.05 level of probability.

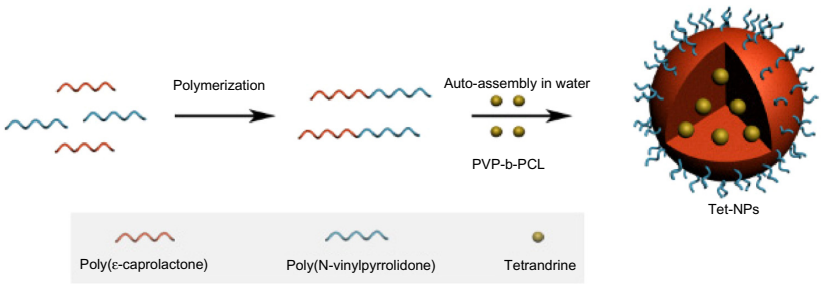

Figure 1 Schematic illustration of synthesis of tetrandrine-loaded PVP-b-PCL nanoparticles.
Abbreviations: PVP-b-PCL, poly(N-vinylpyrrolidone)-block-poly(ε-caprolactone); Tet-NPs, tetrandrine-loaded poly(N-vinylpyrrolidone)-block-poly(ε-caprolactone) nanoparticles.

Results and discussion

Characterization of Tet-NPs

As reported in a previous study, the PVP-hydroxide (OH) was first synthesized and then used as a macromolecular initiator to synthesize a PVP-b-PCL diblock copolymer by ring-opening polymerization of ε-caprolactone (ε-CL). Characterization of PVP-b-PCL by gel permeation chromatography and proton nuclear magnetic resonance (^{1}H-NMR) was described in our previous report.[35] Then Tet-NPs were prepared by a nanoprecipitation method. PVP is at the outside of the nanoparticle as a hydrophilic part while PCL is at the center of the nanoparticle as a hydrophobic part. PVP-b-PCL and Tet can be dissolved in acetone to produce a homogenous and clear solution. Slowly dropping the organic phase into the water phase precipitated the water-insoluble Tet immediately and simultaneously induced a rapid precipitation of the hydrophobic PCL block of the PVP-b-PCL diblock copolymer, resulting in spontaneous formation of Tet-entrapped PVP-b-PCL nanoparticles. The stable Tet-loaded PVP-b-PCL nanoparticle aqueous dispersion was then obtained after the acetone was removed by dialysis (Figure 1).

As part of our current research, different feeding ratios were adopted to study the characteristics of Tet-NPs, including sizes, zeta potentials, and the drug loading efficiencies. As shown in Table 1, three kinds of Tet feeding ratios showed almost no significant influence on size and zeta potential, while influencing drug-loading content and encapsulation efficiency of Tet-NPs. The mean diameters of Tet-NPs were between 110 and 125 nm (Figure 2 and Table 1). The size of lyophilized Tet-NPs was around 140–150 nm, which is a litter larger than that of non-lyophilized Tet-NPs. All four kinds of nanoparticles exhibited a negative zeta potential slightly below 0 mV (Table 1). In addition, a 40% feeding ratio of Tet yielded the highest drug loading content (27.4%) with the lowest encapsulation efficiency (>80%). However, the drug loading content and encapsulation efficiency of a 20% feeding ratio was 15.2% and 89.3%, respectively, which remained the median among the three kinds of nanoparticles (Table 1). In subsequent in vitro release studies, all three types of Tet-NPs showed a controlled release pattern. A 20% feeding ratio of Tet had the most sustained release curve (Figure 3). The release profile of Tet from the lyophilized nanoparticles remained similar to that of non-lyophilized particles, which means lyophilization did not affect the release profile of Tet-NPs. However, the release of Tet-NPs in serum is more accelerated (Figure S1). Therefore, the PVP-b-PCL nanoparticles with a Tet feeding ratio of 20% were used in subsequent experiments to achieve the optimal balance between nanoparticle stability and drug loading efficiency.

Table 1 Characterization of Tet-NPs with different drug feeding

Tet feeding (copolymer based w/w)	Size (nm)[a]/PDI	Zeta potential (mV)	DLC (%)	EE (%)
0	125.3±7.3/0.13	−3.8±0.5	N/A	N/A
10%	115.5±6.9/0.14	−4.5±0.4	9.3±2.1	91.2±5.1
20%	120.2±8.2/0.13	−5.6±1.1	15.2±3.5	89.3±7.3
40%	111.4±9.2/0.14	−6.2±1.2	27.4±4.2	83.2±5.9

Note: [a]Mean diameter was measured by dynamic light scattering.
Abbreviations: Tet-NPs, tetrandrine-loaded poly(N-vinylpyrrolidone)-block-poly (ε-caprolactone) nanoparticles; PDI, polydispersity index; DLC, drug loading content; EE, encapsulation efficiency; Tet, tetrandrine.

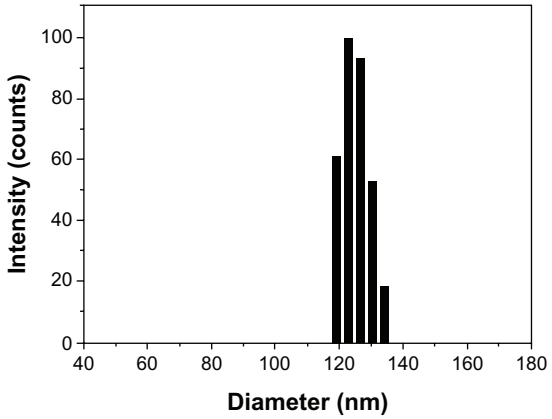

Figure 2 Size distribution of Tet-NPs detected by DLS.
Abbreviations: Tet-NPs, tetrandrine-loaded poly(N-vinylpyrrolidone)-block-poly(ε-caprolactone) nanoparticles; DLS, dynamic light scattering.

Cellular uptake of Tet-NPs by A549 cells

As shown in Figure 4A, after 2 hours incubation with A549 cells at 37°C, Tet-NPs with coumarin-6 inside as

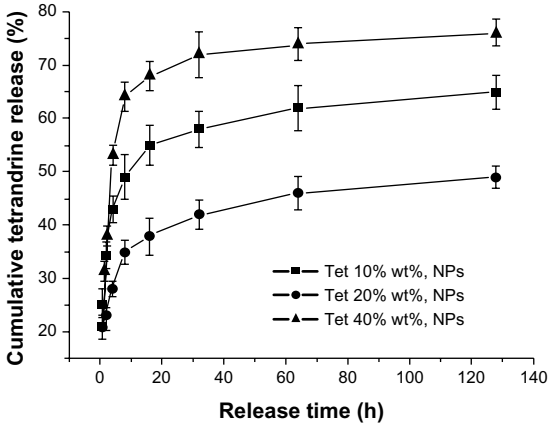

Figure 3 Release curves of Tet-NPs at different feeding ratios.
Abbreviations: Tet-NPs, tetrandrine-loaded poly(N-vinylpyrrolidone)-block-poly (ε-caprolactone) nanoparticles; NPs, nanoparticles; h, hours; wt, weight; Tet, tetrandrine.

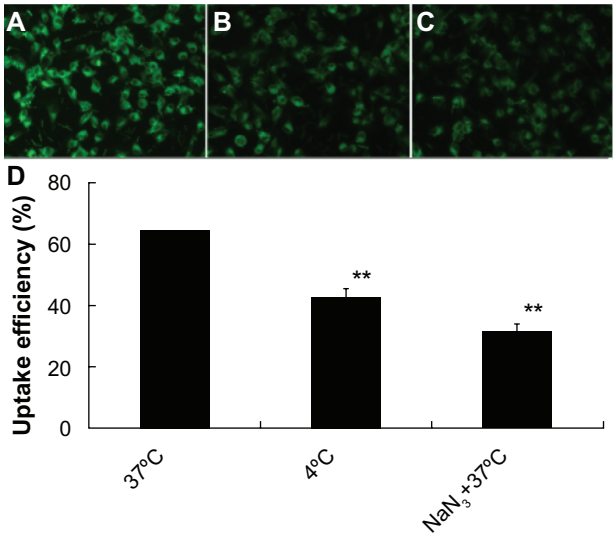

Figure 4 Fluorescent microscope images of A549 cells incubated with coumarin-6-loaded Tet-NPs.
Notes: (**A**) Cells incubated with coumarin-6 loaded Tet-NPs at 37°C. (**B**) Cells incubated with coumarin-6 loaded Tet-NPs at 4°C. (**C**) Cells incubated with both coumarin-6 loaded Tet-NPs and NaN_3 at 37°C. Magnification =400X. (**D**) The cellular uptake efficiency of coumarin-6 loaded Tet-NPs detected by HPLC. **Represents $P<0.01$ versus control.
Abbreviations: Tet-NPs, tetrandrine-loaded poly(N-vinylpyrrolidone)-block-poly(ε-caprolactone) nanoparticles; NaN_3, sodium azide; HPLC, high-performance liquid chromatography.

a fluorescent indicator were transported into A549 cells through endocytosis and the fluorescent dye coumarin-6 located mainly in the cytoplasm. On the contrary, less fluorescence was observed when cells were incubated with fluorescent Tet-NPs for 2 hours at 4°C, which means the process of endocytosis was significantly inhibited at lower temperatures (Figure 4B). In addition, NaN_3, a mitochondrial inhibitor which can inhibit the endocytic process, was used to examine its influence on the cellular uptake efficiency of coumarin-6-loaded Tet-NPs.[37] A549 cells exposed to 20 μM NaN_3 (Figure 4C) showed obviously diminished fluorescence compared to control cells. Quantitative analysis indicated that the uptake efficiency of A549 cells without the presence of NaN_3 at 37°C was more than 60% of the total coumarin-6. However, lower temperature or co-incubation with NaN_3 significantly decreased the uptake efficiency of Tet-NPs (Figure 4D). For instance, the uptake efficiency at 4°C was less than 45%, while 20 mM NaN_3 led to a more than 30% reduction in the uptake efficiency ($P<0.05$ versus control) (Figure 4D).

Therefore, cellular uptake of nanoparticles by A549 cells depends mainly on endocytosis. This endocytic process can be significantly influenced by temperature and blocked by the endocytosis inhibitor NaN_3.[38] It is demonstrated in both our current and previous studies that the uptake of Tet-NPs is mainly mediated by endocytosis, a kind of transportation mechanism which is more efficient than the cellular uptake of free drug by filtration, thereby leading to the enhanced cytotoxicity of Tet-NPs.[25]

Enhanced apoptotic induction of Tet-NPs in A549 cells through inhibition of anti-apoptotic proteins

Two methods were applied to detect the apoptotic rate of A549 cells exposed to a series of doses of Tet-NPs or free Tet. First, there is a simple and rapid way to detect apoptosis qualitatively with fluorescence light microscopy depending on the different uptake of fluorescent deoxyribonucleic acid (DNA) binding dye (such as AO staining).[39] AO can penetrate cell membrane and stain the cell nucleus green.[40] Therefore, it is obvious that live cells have a normal green nucleus while apoptotic cells appear to have a bright green nucleus with distinctive condensed or fragmented chromatin.[41] As shown in Figure 5, compared with free Tet, Tet-NPs induced more apoptosis in A549 cells than free Tet.

Second, the apoptotic rate was quantified by fluorescent Annexin-V-FITC/PI double staining with flow cytometry. Annexin-V specifically recognized the cells entering apoptosis that express phosphatidylserine on the outer layer of the cell membrane. Counterstaining by PI allows the discrimination of apoptotic from necrotic cells. Necrotic cells can be stained only with PI, whereas early apoptotic cells are stained with annexin V and late apoptotic cells can be stained with both annexin V and PI.[42] In our preliminary study, empty

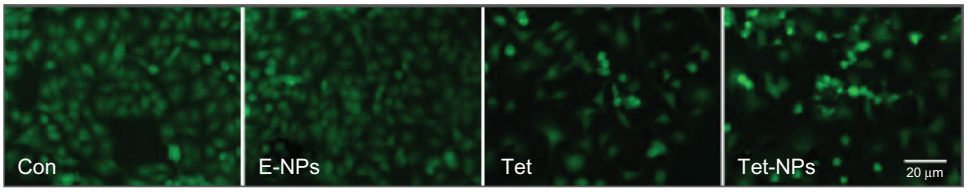

Figure 5 AO staining of A549 cells by fluorescent microscopy exposed to different agents including E-NPs, Tet and Tet-NPs.
Abbreviations: AO, acridine orange; E-NPs, empty nanoparticles; Tet, tetrandrine; Tet-NPs, tetrandrine-loaded poly(N-vinylpyrrolidone)-block-poly(ε-caprolactone) nanoparticles; Con, control.

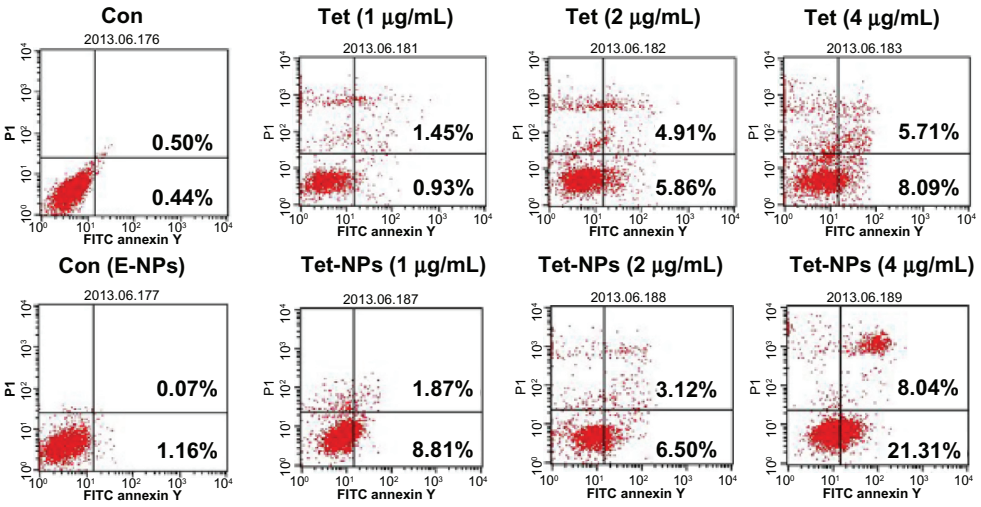

Figure 6 Apoptosis rates induced by a series of doses of Tet or Tet-NPs by FACS.
Abbreviations: Tet, tetrandrine; Tet-NPs, tetrandrine-loaded poly(N-vinylpyrrolidone)-block-poly(ε-caprolactone) nanoparticles; FACS, fluorescence activated cell sorting; Con, control; FITC, fluorescein isothiocyanate; E-NPs, empty nanoparticles.

nanoparticles showed little toxicity to A549 cells, with the cell viability at more than 90%, even at a higher dose of 400 μg/mL (data not shown). Figure 6 indicates that both Tet and Tet-NPs dose-dependently induced apoptosis in A549 cells. It is noted that both early and late apoptosis rates were significantly higher in cells exposed to Tet-NPs when compared to cells exposed to the equivalent doses of free Tet. For example, 21.31% of cells were in the early apoptosis phase when exposed to an equivalent dose of 4 μg/mL Tet-NPs. In contrast, only 8.09% of cells underwent early apoptosis when exposed to free Tet at the same dose. Similarly, 8.81% and 0.93% of cells were entering early apoptosis when they were exposed to Tet-NPs and free Tet at the equivalent dose of 1 μg/mL, respectively.

It has been reported that carcinogenesis results from the misbalance between cell proliferation and apoptosis.[43,44] Growing evidence has demonstrated that the Bcl-2 family, including pro-apoptotic proteins (eg, Bax, Bak, and Bim) and anti-apoptotic proteins (eg, Bcl-2 and Bcl-xL), plays an important role in apoptosis.[45,46] The expression of Bcl-2 and Bax is important in the balance of pro-apoptotic and anti-apoptotic signals at the mitochondrial level.[47] In the current study, we examined the expression of anti-apoptotic proteins in cells exposed to both Tet-NPs and Tet at an equivalent dose of 4 μg/mL. Bcl-2 and Bcl-xL were significantly attenuated by the effect of Tet-NPs and free Tet (Figure 7). Semi-quantification analysis from the image indicated that there is a significant difference in Bcl-2 expression between cells exposed to Tet-NPs and Tet. Tet-NPs decreased expression of Bcl-2 by more than 60%, while free Tet induced a less than 40% reduction, when compared to untreated cells. The same tendency could be observed in the expression of Bcl-xL (Figure 8).

The current data supports that, by inhibiting the expression of anti-apoptotic Bcl-2 and Bcl-xL proteins, Tet-NPs could more efficiently induce the apoptosis of A549 cells than free Tet. The possible mechanism underlying the superior pro-apoptotic effects of Tet-NPs may include the different ways it is transported into cells. As demonstrated in our previous studies, cellular uptake of nanoparticles is mediated by endocytosis, which penetrates cell membranes more efficiently than the infiltration of small molecules.[24–26,48,49] Therefore, cellular uptake of Tet-NPs mediated by endocytosis leads to more intracellular Tet accumulation, thereby more effectively regulating the

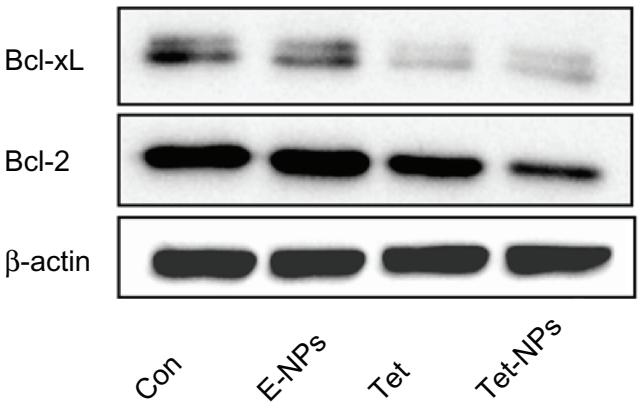

Figure 7 The expression of anti-apoptotic protein Bcl-2 and Bcl-xL in A549 cells exposed to an equivalent dose of Tet or Tet-NPs detected by Western blot analysis.
Abbreviations: Con, control; E-NPs, empty nanoparticles; Tet, tetrandrine; Tet-NPs, tetrandrine-loaded poly(N-vinylpyrrolidone)-block-poly(ε-caprolactone) nanoparticles.

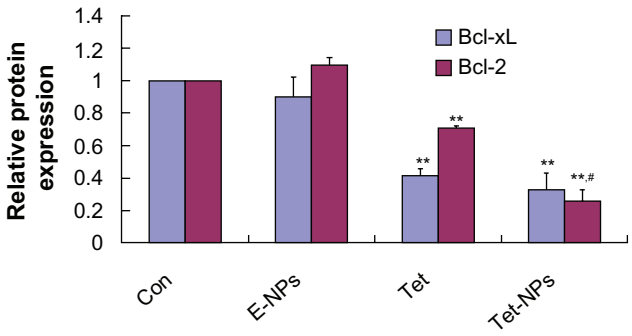

Figure 8 Semi-quantification of the gel image, normalized to β-actin control.
Notes: **Represents $P<0.01$ versus control; #represents $P<0.05$ versus the equivalent dose of Tet (n=3).
Abbreviations: Con, control; E-NPs, empty nanoparticles; Tet, tetrandrine; Tet-NPs, tetrandrine-loaded poly(N-vinylpyrrolidone)-block-poly(ε-caprolactone) nanoparticles.

expression of apoptosis-related proteins and resulting in more apoptosis.

Superior inhibitory effect of Tet-NPs on the migration and invasion of A549 cells by regulating the expression of MMPs

Tumor invasion and metastasis, characteristic of malignancy, remains the leading cause of death in patients suffering from lung cancer.[1] Effective inhibition of tumor invasion and metastasis is seen as a promising way of delaying tumor growth.[50] It is known that tumor invasion and metastasis is a multi-step gradual process with certain procedures, including degradation of ECM, penetration through the vascular endothelial cells, intravascular circulation, and adhesion elsewhere.[51,52] In the whole process, the ability of cell migration and invasion contributes most to tumor growth.[53,54]

Here we chose A549 cells as a model due to their potential to be highly invasive and penetrating. Wound scratching and Transwell assay were adopted to measure the inhibitory effect of Tet-NPs on cell migration and invasion. The expression of MMPs – key proteins in tumor metastasis – were then evaluated by Western blotting.

Figure 9 shows that both Tet-NPs and Tet inhibit the migration of A549 cells in a dose- and time-dependent manner. Moreover, Tet-NPs more efficiently slowed down the migration of A549 cells than free Tet did in the corresponding group, with a significant difference ($P<0.05$) (Figure 10). Quantitative analysis suggests that the wound healing rates of Tet-NPs were significantly lower than that of free Tet at the equivalent dose and time ($P<0.01$) (Figure 10).

Transwell assay was performed to evaluate the invasive ability of A549 cells exposed to Tet-NPs and free Tet. An invasion chamber kit (Becton, Dickinson and Company) with a Matrigel-coated filter in the chamber was applied to stimulate the invasion of tumor cells across the ECM. Figure 11 shows that the successfully invading cells (crystal-violet staining) decreasing as the drug concentration increases, suggesting the dose-dependent inhibitory effect of Tet-NPs or Tet on the invasive ability of A549 cells. Most importantly, there is a significant difference in the number of invading cells between the group of Tet-NPs and Tet ($P<0.01$); this demonstrates the superior inhibitory effect of Tet-NPs on invasion when compared with an equivalent dose of Tet (Figure 12).

Data from wound scratch and Transwell assays suggests that delivery of Tet in PVP-b-PCL nanoparticles restrains the mobility of A549 cells more effectively than free Tet. It is demonstrated that the degradation of the ECM, which is crucial for tumor cell invasion, depends mainly on the activity of matrix-degrading proteinases, such as MMP-2 and MMP-9, as well as TIMP-3, the inhibitor of MMPs.[55–57] To further study the inhibitory effect of Tet-NPs on tumor invasion and metastasis, the activity of MMPs was detected (Figures 13 and 14). The expression of MMP-2 and MMP-9, which are the main proteinases

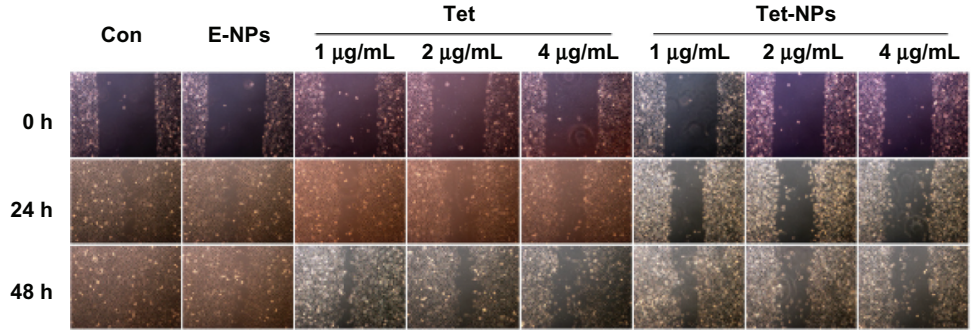

Figure 9 Wound healing ability of A549 cells exposed to equivalent doses of Tet or Tet-NPs. Phase micrograph of A549 cells at various time points after monolayer wounding.
Abbreviations: Con, control; E-NPs, empty nanoparticles; Tet, tetrandrine; Tet-NPs, tetrandrine-loaded poly(N-vinylpyrrolidone)-block-poly(ε-caprolactone) nanoparticles; h, hours.

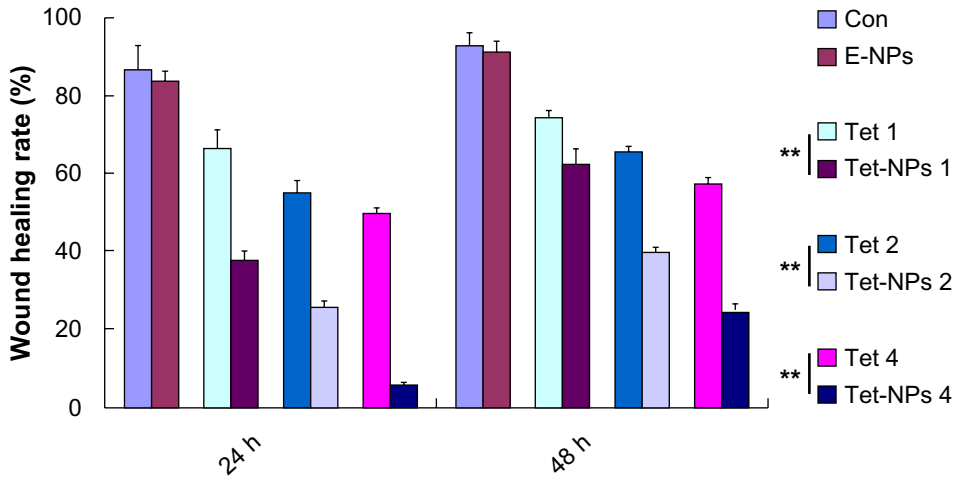

Figure 10 Quantification of cell migration using the monolayer wound scratching assay.
Notes: **Represents $P<0.01$ versus the equivalent dose of Tet. Each data point represents the mean ± SD from three independent experiments.
Abbreviations: Con, control; E-NPs, empty nanoparticles; Tet, tetrandrine; Tet-NPs, tetrandrine-loaded poly(N-vinylpyrrolidone)-block-poly(ε-caprolactone) nanoparticles; h, hours; SD, standard deviation.

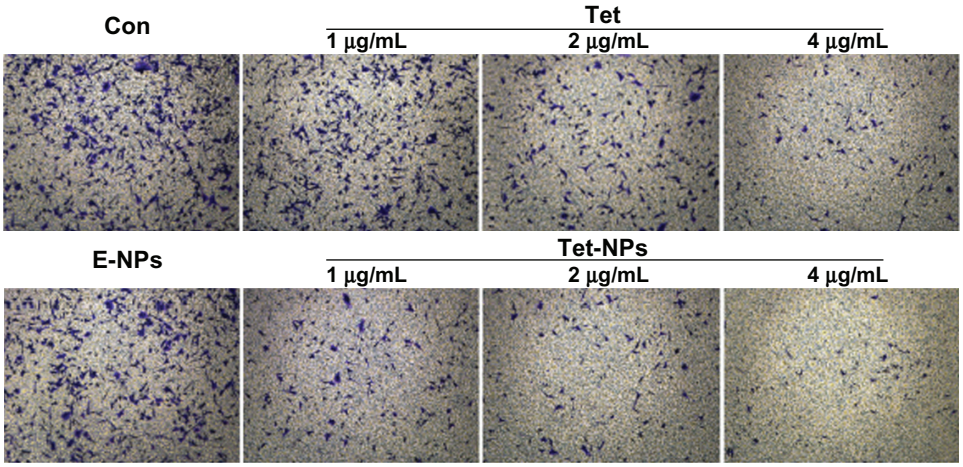

Figure 11 Cell invasive ability of A549 cells exposed to equivalent doses of Tet or Tet-NPs.
Notes: A549 cells were treated with Tet or Tet-NPs at equivalent doses of 0, 1, 2, and 4 μg/mL for 48 hours. Invading cells were fixed with methanol, stained with crystal violet, and photographed under fluorescent microscopy.
Abbreviations: Con, control; E-NPs, empty nanoparticles; Tet, tetrandrine; Tet-NPs, tetrandrine-loaded poly(N-vinylpyrrolidone)-block-poly(ε-caprolactone) nanoparticles.

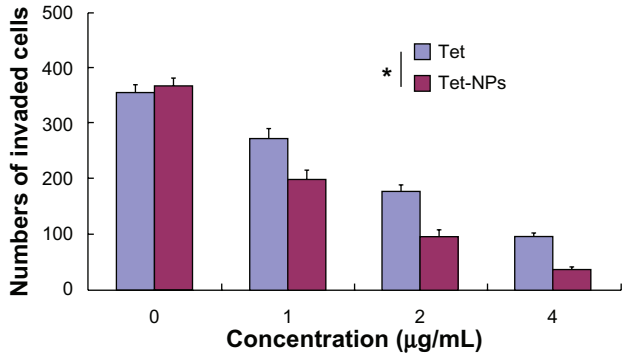

Figure 12 Quantification of cell invasion.
Notes: Each data point represents the mean ± SD from three independent experiments; *represents $P<0.05$ versus equivalent doses of Tet.
Abbreviations: SD, standard deviation; Tet, tetrandrine; Tet-NPs, tetrandrine-loaded poly(N-vinylpyrrolidone)-block-poly(ε-caprolactone) nanoparticles.

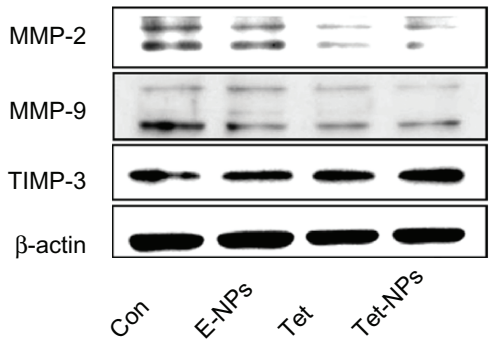

Figure 13 The expression of metastatic relative protein MMP-2, MMP-9 and TIMP-3 in A549 cells exposed to an equivalent dose of Tet or Tet-NPs.
Abbreviations: MMP, matrix metalloproteinase; TIMP-3, tissue inhibitor of MMP-3; Con, control; E-NPs, empty nanoparticles; Tet, tetrandrine; Tet-NPs, tetrandrine-loaded poly(N-vinylpyrrolidone)-block-poly(ε-caprolactone) nanoparticles.

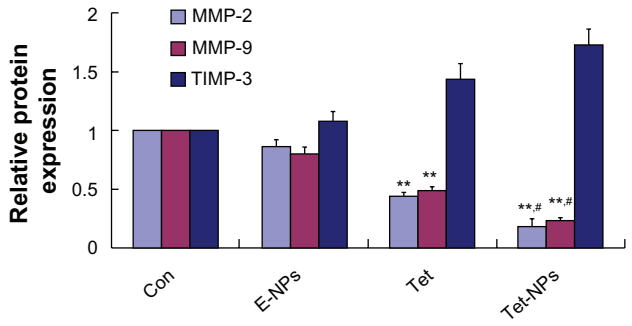

Figure 14 Semi-quantification of the gel image, normalized to β-actin control.
Notes: **Represents $P<0.01$ versus control; #represents $P<0.05$ versus the equivalent dose of Tet (n=3).
Abbreviations: MMP, matrix metalloproteinase; TIMP-3, tissue inhibitor of MMP-3; Con, control; E-NPs, empty nanoparticles; Tet, tetrandrine; Tet-NPs, tetrandrine-loaded poly(N-vinylpyrrolidone)-block-poly(ε-caprolactone) nanoparticles.

degrading the ECM, was significantly attenuated by both Tet-NPs and Tet, when compared to control group (Figure 12). Moreover, significant differences ($P<0.05$) were observed; nearly 80% of the MMP-2 and MMP-9 expression was inhibited by Tet-NPs, while a decrease of less than 60% of the expression was detected in cells exposed to the equivalent dose of Tet. In addition, TIMP-3, the inhibitor of MMPs, increased more significantly in cells treated with Tet-NPs than in those treated with free Tet (Figure 14).

Conclusion

The current study reported a simple way of preparing drug-loaded nanoparticles formed by combining amphiphilic PVP-b-PCL copolymers and Tet as a model drug. A Trojan strategy of Tet delivery by PVP-b-PCL nanoparticle endocytosis leads to enhanced apoptosis induction in A549 cells; this is achieved by inhibiting the expression of anti-apoptotic Bcl-2 and Bcl-xL proteins. Furthermore, Tet-NPs more efficiently inhibit the ability of cell migration and invasion than free Tet by down-regulating MMP-2 and MMP-9, as well as up-regulating TIMP-3. Therefore, data from this study not only confirm the potential of Tet in treating lung cancer but also offer an effective way to improve the anticancer efficiency of Tet by nanodrug delivery systems. This proposal enriches the current research being carried out on the drug delivery systems in treating lung cancer and documents additional research data, which we can contribute.

Acknowledgments

This work was supported by the following: the National Natural Science Foundation of China (81101902 to H Xu, 81273571 to W Xie); the National Major Scientific and Technological Special Project for "Significant New Drugs Development" (2011ZX09302-003-02); the Jiangsu Province Major Scientific and Technological Special Project (BM2011017); a project funded by the Priority Academic Program Development of Jiangsu Higher Education Institutions (PAPD). We thank Ms Denis Jennings for proofreading.

Disclosure

The authors report no conflicts of interest in this work.

References

1. Siegel R, Naishadham D, Jemal A. Cancer statistics, 2013. *CA Cancer J Clin.* 2013;63(1):11–30.
2. Shawihdi M, Thompson E, Kapoor N, et al. Variation in gastroscopy rate in English general practice and outcome for oesophagogastric cancer: retrospective analysis of Hospital Episode Statistics. *Gut.* Epub February 20, 2013.
3. Rami-Porta R, Crowley JJ, Goldstraw P. The revised TNM staging system for lung cancer. *Ann Thorac Cardiovasc Surg*. 2009;15(1):4–9.
4. Rami-Porta R, Bolejack V, Goldstraw P. The new tumor, node, and metastasis staging system. *Semin Respir Crit Care Med.* 2011;32(1):44–51.
5. Oh SH, Lee BH. Induction of apoptosis in human hepatoblastoma cells by tetrandrine via caspase-dependent Bid cleavage and cytochrome c release. *Biochem Pharmacol*. 2003;66(5):725–731.
6. Kuo PL, Lin CC. Tetrandrine-induced cell cycle arrest and apoptosis in Hep G2 cells. *Life Sci.* 2003;73(2):243–252.
7. Yu VW, Ho WS. Tetrandrine inhibits hepatocellular carcinoma cell growth through the caspase pathway and G2/M phase. *Oncol Rep.* 2013;29(6):2205–2210.
8. Chen T, Ji B, Chen Y. Tetrandrine triggers apoptosis and cell cycle arrest in human renal cell carcinoma cells. *J Nat Med*. Epub April 6, 2013.
9. Wan J, Liu T, Mei L, et al. Synergistic antitumour activity of sorafenib in combination with tetrandrine is mediated by reactive oxygen species (ROS)/Akt signaling. *Br J Cancer*. 2013;109(2):342–350.
10. Qian X, Yan B, Zhou X, et al. Synergistic antiangiogenic activity of tetrandrine combined with Endostar on the human umbilical vein endothelial cell model. *Cancer Biother Radiopharm*. 2013;28(5):385–390.
11. Dai CL, Xiong HY, Tang LF, et al. Tetrandrine achieved plasma concentrations capable of reversing MDR in vitro and had no apparent effect on doxorubicin pharmacokinetics in mice. *Cancer Chemother Pharmacol*. 2007;60(5):741–750.
12. Wei J, Liu B, Wang L, Qian X, Ding Y, Yu L. Synergistic interaction between tetrandrine and chemotherapeutic agents and influence of tetrandrine on chemotherapeutic agent-associated genes in human gastric cancer cell lines. *Cancer Chemother Pharmacol*. 2007;60(5):703–711.
13. Sebens S, Schafer H. The tumor stroma as mediator of drug resistance – a potential target to improve cancer therapy? *Curr Pharm Biotechnol.* 2012;13(11):2259–2272.
14. Herszényi L, Hritz I, Lakatos G, Varga MZ, Tulassay Z. The behavior of matrix metalloproteinases and their inhibitors in colorectal cancer. *Int J Mol Sci*. 2012;13(10):13240–13263.
15. Rollin J, Régina S, Vourc'h P, et al. Influence of MMP-2 and MMP-9 promoter polymorphisms on gene expression and clinical outcome of non-small cell lung cancer. *Lung Cancer.* 2007;56(2):273–280.
16. Chang KH, Liao HF, Chang HH, et al. Inhibitory effect of tetrandrine on pulmonary metastases in CT26 colorectal adenocarcinoma-bearing BALB/c mice. *Am J Chin Med*. 2004;32(6):863–872.
17. Gao JL, Ji X, He TC, et al. Tetrandrine suppresses cancer angiogenesis and metastasis in 4t1 tumor bearing mice. *Evid Based Complement Alternat Med*. 2013;2013:265061.

18. Li S, Ji Z, Zou M, Nie X, Shi Y, Cheng G. Preparation, characterization, pharmacokinetics and tissue distribution of solid lipid nanoparticles loaded with tetrandrine. *AAPS Pharm Sci Tech.* 2011;12(3):1011–1018.
19. Sadeghi-Aliabadi H, Mozaffari M, Behdadfar B, Raesizadeh M, Zarkesh-Esfahani H. Preparation and cytotoxic evaluation of magnetite (Fe_3O_4) nanoparticles on breast cancer cells and its combinatory effects with doxorubicin used in hyperthermia. *Avicenna J Med Biotechnol*. 2013;5(2):96–103.
20. Li R, Li X, Xie L, et al. Preparation and evaluation of PEG-PCL nanoparticles for local tetradrine delivery. *Int J Pharm*. 2009;379(1): 158–166.
21. Chen B, Sun Q, Wang X, et al. Reversal in multidrug resistance by magnetic nanoparticle of Fe_3O_4 loaded with adriamycin and tetrandrine in K562/A02 leukemic cells. *Int J Nanomedecine.* 2008;3(2):277–286.
22. Cheng J, Wu W, Chen BA, et al. Effect of magnetic nanoparticles of Fe_3O_4 and 5-bromotetrandrine on reversal of multidrug resistance in K562/A02 leukemic cells. *Int J Medecine.* 2009;4:209–216.
23. Li R, Xie L, Zhu Z, et al. Reversion of pH-induced physiological drug resistance: a novel function of copolymeric nanoparticles. *PloS One.* 2011;6(9):e24172.
24. Li X, Xu H, Dai X, Zhu Z, Liu B, Lu X. Enhanced in vitro and in vivo therapeutic efficacy of codrug-loaded nanoparticles against liver cancer. *Int J Nanomedecine.* 2012;7:5183–5190.
25. Li X, Zhen D, Lu X, et al. Enhanced cytotoxicity and activation of ROS-dependent c-Jun NH2-terminal kinase and caspase-3 by low doses of tetrandrine-loaded nanoparticles in Lovo cells – a possible Trojan strategy against cancer. *Eur J Pharm Biopharm.* 2010;75(3):334–340.
26. Li X, Lu X, Xu H, et al. Paclitaxel/tetrandrine coloaded nanoparticles effectively promote the apoptosis of gastric cancer cells based on "oxidation therapy". *Mol Pharm.* 2012;9(2):222–229.
27. Ding D, Li K, Qin W, et al. Conjugated polymer amplified far-red/near-infrared fluorescence from nanoparticles with aggregation-induced emission characteristics for targeted in vivo imaging. *Adv Healthcare Mater.* 2013;2(3):500–507.
28. Ding D, Li K, Zhu Z, et al. Conjugated polyelectrolyte-cisplatin complex nanoparticles for simultaneous in vivo imaging and drug tracking. *Nanoscale.* 2011;3(5):1997–2002.
29. Ding D, Zhu Z, Li R, et al. Nanospheres-incorporated implantable hydrogel as a trans-tissue drug delivery system. *ACS Nano.* 2011;5(4): 2520–2534.
30. Ding D, Wang J, Zhu Z, et al. Tumor accumulation, penetration, and antitumor response of cisplatin-loaded gelatin/poly(acrylic acid) nanoparticles. *ACS Appl Mater Interfaces.* 2012;4(3):1838–1846.
31. Ding D, Zhu Z, Liu Q, et al. Cisplatin-loaded gelatin-poly(acrylic acid) nanoparticles: synthesis, antitumor efficiency in vivo and penetration in tumors. *Eur J Pharm Biopharm*. 2011;79(1):142–149.
32. Ishida T, Ichihara M, Wang X, et al. Injection of PEGylated liposomes in rats elicits PEG-specific IgM, which is responsible for rapid elimination of a second dose of PEGylated liposomes. *J Control Release*. 2006;112(1):15–25.
33. Leiva A, Quina FH, Araneda E, Gargallo L, Radic D. New three-arm amphiphilic and biodegradable block copolymers composed of poly(epsilon-caprolactone) and poly(N-vinyl-2-pyrrolidone). Synthesis, characterization and self-assembly in aqueous solution. *J Colloid Interface Sci*. 2007;310(1):136–143.
34. Kaneda Y, Tsutsumi Y, Yoshioka Y, et al. The use of PVP as a polymeric carrier to improve the plasma half-life of drugs. *Biomaterials.* 2004;25(16):3259–3266.
35. Zhu Z, Li Y, Li X, et al. Paclitaxel-loaded poly(N-vinylpyrrolidone)-b-poly(epsilon-caprolactone) nanoparticles: preparation and antitumor activity in vivo. *J Control Release*. 2010;142(3):438–446.
36. Li X, Li R, Qian X, et al. Superior antitumor efficiency of cisplatin-loaded nanoparticles by intratumoral delivery with decreased tumor metabolism rate. *Eur J Pharm Biopharm*. 2008;70(3):726–734.
37. Schmid SL, Carter LL. ATP is required for receptor-mediated endocytosis in intact cells. *J Cell Biol*. 1990;111(6 Pt 1):2307–2318.
38. Kim JS, Yoon TJ, Yu KN, et al. Cellular uptake of magnetic nanoparticle is mediated through energy-dependent endocytosis in A549 cells. *J Vet Sci*. 2006;7(4):321–326.
39. Mpoke SS, Wolfe J. Differential staining of apoptotic nuclei in living cells: application to macronuclear elimination in Tetrahymena. *J Histochem Cytochem*. 1997;45(5):675–683.
40. Ribble D, Goldstein NB, Norris DA, Shellman YG. A simple technique for quantifying apoptosis in 96-well plates. *BMC Biotechnol.* 2005;5:12.
41. Renvoizé C, Biola A, Pallardy M, Bréard J. Apoptosis: identification of dying cells. *Cell Biol Toxicol*. 1998;14(2):111–120.
42. Chen S, Cheng AC, Wang MS, Peng X. Detection of apoptosis induced by new type gosling viral enteritis virus in vitro through fluorescein annexin V-FITC/PI double labeling. *World J Gastroenterol*. 2008;14(14):2174–2178.
43. Williams GT, Smith CA. Molecular regulation of apoptosis: genetic controls on cell death. *Cell.* 1993;74(5):777–779.
44. Öhlund D, Franklin O, Lundberg E, Lundin C, Sund M. Type IV collagen stimulates pancreatic cancer cell proliferation, migration, and inhibits apoptosis through an autocrine loop. *BMC Cancer.* 2013;13:154.
45. Hardwick JM, Chen YB, Jonas EA. Multipolar functions of BCL-2 proteins link energetics to apoptosis. *Trends Cell Biol.* 2012;22(6): 318–328.
46. Adams JM, Cory S. The Bcl-2 protein family: arbiters of cell survival. *Science.* 1998;281(5381):1322–1326.
47. Hetz CA. ER stress signaling and the BCL-2 family of proteins: from adaptation to irreversible cellular damage. *Antioxid Redox Signal*. 2007;9(12):2345–2355.
48. Shao J, Zheng D, Jiang Z, et al. Curcumin delivery by methoxy polyethylene glycol-poly(caprolactone) nanoparticles inhibits the growth of C6 glioma cells. *Acta Biochim Biophys Sin (Shanghai)*. 2011;43(4): 267–274.
49. Lu X, Xu H, Sun B, Zhu Z, Zheng D, Li X. Enhanced neuroprotective effects of resveratrol delivered by nanoparticles on hydrogen peroxide-induced oxidative stress in rat cortical cell culture. *Mol Pharm.* 2013;10(5):2045–2053.
50. Bergers G, Hanahan D. Modes of resistance to anti-angiogenic therapy. *Nat Rev Cancer.* 2008;8(8):592–603.
51. Oskarsson T. Extracellular matrix components in breast cancer progression and metastasis. *Breast.* 2013;22 Suppl 2:S66–S72.
52. Koontongkaew S. The tumor microenvironment contribution to development, growth, invasion and metastasis of head and neck squamous cell carcinomas. *J Cancer.* 2013;4(1):66–83.
53. Valastyan S, Weinberg RA. Tumor metastasis: molecular insights and evolving paradigms. *Cell.* 2011;147(2):275–292.
54. Gupta GP, Massagué J. Cancer metastasis: building a framework. *Cell.* 2006;127(4):679–695.
55. Groblewska M, Siewko M, Mroczko B, Szmitkowski M. The role of matrix metalloproteinases (MMPs) and their inhibitors (TIMPs) in the development of esophageal cancer. *Folia Histochem Cytobiol*. 2012;50(1):12–19.
56. Cook H, Davies KJ, Harding KG, Thomas DW. Defective extracellular matrix reorganization by chronic wound fibroblasts is associated with alterations in TIMP-1, TIMP-2, and MMP-2 activity. *J Invest Dermatol*. 2000;115(2):225–233.
57. Gao ZL, Zhang C, Du GY, Lu ZJ. Clinical significance of changes in tumor markers, extracellular matrix, MMP-9 and VEGF in patients with gastric carcinoma. *Hepatogastroenterology.* 2007;54(77):1591–1595.

Supplementary figure

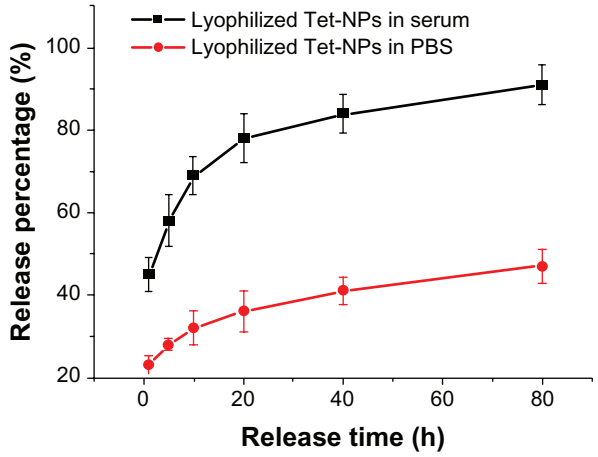

Figure S1 Release curves of lyophilized Tet-NPs in PBS and serum.
Abbreviations: Tet-NPs, tetrandrine-loaded poly(N-vinylpyrrolidone)-block-poly(ε-caprolactone) nanoparticles; PBS, phosphate buffered saline; h, hours.